LANGD5

Langmuir

The ACS Journal of Surfaces and Colloids

APRIL 1, 2008

VOLUME 24, NUMBER 7

http://pubs.acs.org/Langmuir

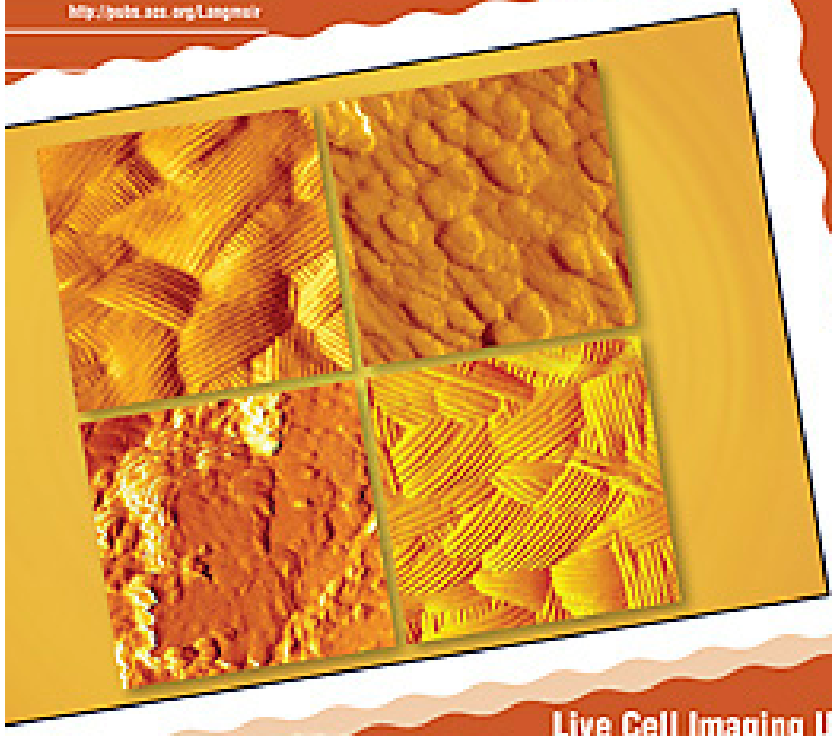

Live Cell Imaging Using Atomic Force Microscopy

(see p. 24A)

Table of Contents

Vol. 24, No. 7: April 1,2008

Combined Use of Atomic Force Microscopy, X-ray Photoelectron Spectroscopy, and Secondary Ion Mass Spectrometry for Cell Surface Analysis

Etienne Dague, Arnaud Delcorte, Jean-Paul Latgé, and Yves F. Dufrêne

pp 2955 - 2959; **(Letter)** DOI: 10.1021/la703741y

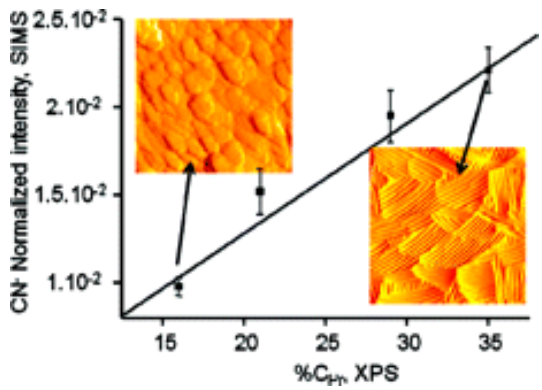

Langmuir
The ACS Journal of Surfaces and Colloids

APRIL 1, 2008
VOLUME 24, NUMBER 7

Letters

Combined Use of Atomic Force Microscopy, X-ray Photoelectron Spectroscopy, and Secondary Ion Mass Spectrometry for Cell Surface Analysis

Etienne Dague,[†] Arnaud Delcorte,[‡] Jean-Paul Latgé,[§] and Yves F. Dufrêne*,[†]

Unité de Chimie des Interfaces, Université Catholique de Louvain, Croix du Sud 2/18, B-1348 Louvain-la-Neuve, Belgium, Unité de Physico-Chimie et Physique des Matériaux, Université Catholique de Louvain, Croix du Sud 1, B-1348 Louvain-la-Neuve, Belgium, and Unité des Aspergillus, Institut Pasteur Paris France, 25 rue du docteur Roux, 75724 Paris, France

Received November 29, 2007. In Final Form: January 11, 2008

Understanding the surface properties of microbial cells is a major challenge of current microbiological research and a key to efficiently exploit them in biotechnology. Here, we used three advanced surface analysis techniques with different sensitivity, probing depth, and lateral resolution, that is, *in situ* atomic force microscopy, X-ray photoelectron spectroscopy, and secondary ion mass spectrometry, to gain insight into the surface properties of the conidia of the human fungal pathogen *Aspergillus fumigatus*. We show that the native ultrastructure, surface protein and polysaccharide concentrations, and amino acid composition of three mutants affected in hydrophobin production are markedly different from those of the wild-type, thereby providing novel insight into the cell wall architecture of *A. fumigatus*. The results demonstrate the power of using multiple complementary techniques for probing microbial cell surfaces.

Introduction

Characterizing the surface properties of microbes is of major importance to understand their behavior at interfaces (i.e., cell adhesion), to fight them in the biomedical context (pathogen-host interactions), and to efficiently exploit them in biotechnology (biofilm formation). During the past decades, much progress has been made in applying surface analysis techniques to microbial surfaces, complementing other biochemical and physical methods. Particularly, X-ray photoelectron spectroscopy (XPS)[1] has been used to determine the surface chemical composition, over a depth of ~5 nm, of a wide variety of microbial cells, including yeast, fungi, and bacteria, in relation to surface properties and adhesion behavior.[2,3] Although very powerful, XPS is limited by its poor lateral resolution, meaning it is not adapted for microbial cell imaging. By contrast, secondary ion mass spectrometry (SIMS)[4−6] has a much higher surface sensitivity, allowing one to probe low levels of biomolecules. Also, because the technique offers a lateral resolution better than 1 μm, it has been successfully used for imaging cells, tissues, and membranes.[7−12] For instance, using a complete cold chain freeze-fracture methodology, time-of-

* To whom correspondence should be addressed. Telephone: (32) 10 47 36 00. Fax: (32) 10 47 20 05. E-mail: dufrene@cifa.ucl.ac.be.
[†] Unité de Chimie des Interfaces, Université Catholique de Louvain.
[‡] Unité de Physico-Chimie et Physique des Matériaux, Université Catholique de Louvain.
[§] Institut Pasteur Paris France.

(1) McArthur, S. L. *Surf. Interface Anal.* **2006**, *38*, 1380.
(2) Rouxhet, P. G.; Mozes, N.; Dengis, P. B.; Dufrêne, Y. F.; Gerin, P. A.; Genet, M. J. *Colloids Surf., B* **1994**, *2*, 347.
(3) Van der Mei, H. C.; Vries, J.; Busscher, H. J. *Surf. Sci. Rep.* **2000**, *39*, 1.
(4) Belu, A. M.; Graham, D. J.; Castner, D. G. *Biomaterials* **2003**, *24*, 3635.
(5) Vickerman, J. C., Briggs, D., Eds. *Surface Spectra*; IM Publications: Chichester, U.K., 2001.
(6) Liam, A.; McDonnell, R. M. A. H. *Mass Spectrom. Rev.* **2007**, *26*, 606.
(7) Colliver, T. L.; Brummel, C. L.; Pacholski, M. L.; Swanek, F. D.; Ewing, A. G.; Winograd, N. *Anal. Chem.* **1997**, *69*, 2225.
(8) Cannon, D. M.; Pacholski, M. L.; Winograd, N.; Ewing, A. G. *J. Am. Chem. Soc.* **2000**, *122*, 603.
(9) Lockyer, N. P.; Vickerman, J. C. *Appl. Surf. Sci.* **2004**, *231−232*, 377.
(10) Ostrowski, S. G.; Van Bell, C. T.; Winograd, N.; Ewing, A. G. *Science* **2004**, *305*, 71.

10.1021/la703741y CCC: $40.75
Published on Web 02/01/2008

flight (ToF)-SIMS imaging could be used to obtain images of molecular species across a cell surface with a submicrometer ion probe beam.[7] Images of small hydrocarbons and the deliberately added dopants dimethyl sulfoxide (DMSO) and cocaine were obtained on the surface of the single cell organism *Paramecium*. In another work, ToF-SIMS images of both frozen-hydrated and freeze-dried microbial cells revealed molecular information for single cells, including components of the cell wall, membrane, and cytoplasm.[9] Combining the approach with principal component analysis (PCA) allowed the classification of yeast cells from different species and strains. Using a combination of ToF-SIMS and PCA, conclusions could also be drawn concerning the change of conformation of proteins at surfaces as a function of the concentration in solution.[13] Notably, the technique has recently been used to analyze the chemical composition of lipid domains in supported lipid membranes, with a lateral resolution of only 100 nm, suggesting that such nano-SIMS approach should find broad applications in future cell surface research.[11] Compared with XPS, the main drawback of SIMS arises from the difficulty to extract quantitative information from the measured signal. Overcoming this issue would require a complete understanding of the fundamentals of the ion−surface interaction,[14] because the mechanisms of molecular desorption, fragmentation, and ionization are influenced in a complex manner by the nature and energy of the projectile and by the environment of the considered analyte (matrix effects).[15] In this context, it is very informative to correlate the SIMS data with results obtained using other surface analysis techniques such as XPS.

Surface analysis techniques such as XPS and SIMS are limited by the requirement of vacuum conditions during the analysis; that is, hydrated live cells cannot be directly investigated. Therefore, complementing these methods with *in situ*, high-resolution imaging techniques is of great interest. Recently, atomic force microscopy (AFM) has shown to be a powerful tool in this respect.[16] The technique not only images the structures of single live cells with nanoscale resolution[16] but also measures their physical[17] and chemical[18] properties and detects individual cell surface receptors.[19]

In this study, we use the combination of AFM, XPS, and SIMS to gain a comprehensive view of the surface properties of the conidia of the human fungal pathogen *Aspergillus fumigatus*. We focused on this microbe in view of its medical importance[20] and because of the availability of mutants affected in cell surface constituents.[21,22] The cell walls of the *A. fumigatus* conidia are covered by a thin layer of regularly arranged rodlets composed of the hydrophobin RodAp, a small hydrophobic protein favoring spore dispersion and adherence to host cells. Another hydrophobin, RodBp, has also been found in the conidium, but its role remains poorly understood. Here, we show that the surface structure (AFM) and surface chemical composition (XPS and SIMS) of *A. fumigatus* mutants markedly differ from those of the wild-type, in agreement with earlier biochemical data. The results provide novel insight into the *A. fumigatus* cell wall organization and demonstrate the power of using the AFM/XPS/SIMS multitechnique approach in microbial genetic studies for assessing the phenotypic characteristics of mutants altered in cell wall constituents.

Materials and Methods

We used the wild-type strain *A. fumigatus* CBS144-89 which is of clinical origin. The ΔrodA and ΔrodB mutants and ΔrodAΔrodB double mutant were obtained previously on the CBS144-89 background.[21,22] Conidia were harvested from 1-week-old cultures grown at 25 °C on 2% malt extract agar. They were recovered in water containing 0.1% Tween20, rinsed three times in tweened water and five times in deionized water, and either directly imaged by AFM or lyophilized for XPS and SIMS analyses.

AFM images were obtained in contact mode at room temperature (20 °C) in deionized water, using a Nanoscope IV Multimode atomic force microscope with oxide-sharpened microfabricated Si_3N_4 cantilevers of 0.01 N/m spring constants (Veeco Metrology Group, Santa Barbara, CA). For live cell imaging, conidia were immobilized by mechanical trapping into polycarbonate porous membranes (Millipore). After filtering a cell suspension (20 mL; 2.5×10^6 cells/mL), the filter was carefully rinsed in deionized water, cut (1 cm × 1 cm), and attached to a steel sample puck using a small piece of adhesive tape, and then the mounted sample was transferred into the AFM liquid cell. The imaging force was kept as low as possible (∼250 pN) to minimize sample damage.

X-ray photoelectron spectroscopy (XPS) analyses were performed on a Kratos Axis Ultra spectrometer (Kratos Analytical, U.K.) equipped with a monochromatized aluminum X-ray source. The angle between the normal to the sample surface and the electrostatic lens axis was 0°. The analyzed area was ∼700 μm × 300 μm. The constant pass energy of the hemispherical analyzer was set at 40 eV. The following sequence of spectra was recorded: survey spectrum, C_{1s}, N_{1s}, O_{1s}, and C_{1s} again to check the stability of charge compensation as a function of time and the absence of degradation of the sample during the analyses. The binding energies were calculated with respect to the *C*−(C,H) component of the C1s peak of adventitious carbon fixed at 284.8 eV. Following subtraction of a linear baseline, molar fractions were calculated (CasaXPS program, Casa Software Ltd., U.K.) using peak areas normalized on the basis of acquisition parameters, sensitivity factors, and the transmission function provided by the manufacturer.

The time-of-flight secondary ion mass spectrometry (ToF-SIMS) analyses were performed in a Phi-Evans TFS-4000MMI (TRIFT 1) spectrometer.[23,24] The samples were pressed on a silver tape, covered with a stainless steel grid for charge compensation, and mechanically mounted on the sample holder. A pulsed 15 keV gallium ion beam (∼1200 pA direct current, 8 kHz pulsing frequency, 22 ns pulse width bunched down to 1 ns) was rastered over a 120 μm × 120 μm area for an acquisition time of 180 s. The total fluence per spectrum was about 1.65×10^{12} ions/cm^2, which ensured static analysis conditions. The secondary ions were accelerated to 3 keV and focused by two lenses before undergoing a 270° deflection in three hemispherical electrostatic analyzers. A 7 keV postacceleration was applied at the detector entry to increase the detection efficiency of high-mass ions. The charge compensation was performed using a pulsed electron beam (24 eV) and a nonmagnetic stainless steel grid placed on each sample. The mass resolution ($m/\Delta m$) at $m/z =$ 41 was always larger than 3000 and, therefore, sufficient to resolve multiple peaks with the same nominal mass. For each sample, three spectra were recorded at different areas to check the reproducibility.

(11) Kraft, M. L.; Weber, P. K.; Longo, M. L.; Hutcheon, I. D.; Boxer, S. G. *Science* **2006**, *313*, 1948.
(12) Fletcher, J. S.; Lockyer, N. P.; Vaidyanathan, S.; Vickerman, J. C. *Anal. Chem.* **2007**, *79*, 2199.
(13) Henry, M.; Dupont-Gillain, C.; Bertrand, P. *Langmuir* **2003**, *19*, 6271.
(14) Delcorte, A. *Phys. Chem. Chem. Phys.* **2005**, *7*, 3395.
(15) Delcorte, A. *Appl. Surf. Sci.* **2006**, *252*, 6582.
(16) Dufrêne, Y. F. *Nat. Rev. Microbiol.* **2004**, *2*, 451.
(17) Gaboriaud, F.; Bailet, S.; Dague, E.; Jorand, F. *J. Bacteriol.* **2005**, *187*, 3864.
(18) Alsteens, D.; Dague, E.; Rouxhet, P. G.; Baulard, A. R.; Dufrene, Y. F. *Langmuir* **2007**, *23*, 11977.
(19) Dupres, V.; Menozzi, F. D.; Locht, C.; Clare, B. H.; Abbott, N. L.; Cuenot, S.; Bompard, C.; Raze, D.; Dufrêne, Y. F. *Nat. Methods* **2005**, *2*, 515.
(20) Maubon, D.; Park, S.; Tanguy, M.; Huerre, M.; Schmitt, C.; Prevost, M. C.; Perlin, D. S.; Latge, J. P.; Beauvais, A. *Fungal Genet. Biol.* **2006**, *43*, 366.
(21) Thau, N.; Monod, M.; Crestani, B.; Rolland, C.; Tronchin, G.; Latge, J. P.; Paris, S. *Infect. Immun.* **1994**, *62*, 4380.
(22) Paris, S.; Debeaupuis, J.-P.; Crameri, R.; Carey, M.; Charlès, F.; Prévost, M. C.; Schmitt, C.; Philippe, B.; Latgé, J. P. *Appl. Environ. Microbiol.* **2003**, *69*, 1581.
(23) Bertrand, P.; Weng, L. T. *Mikrochim. Acta Suppl.* **1996**, *13*, 167.
(24) Schueler, B. W. *Microsc. Microanal. Microstruct.* **1992**, *3*, 119.

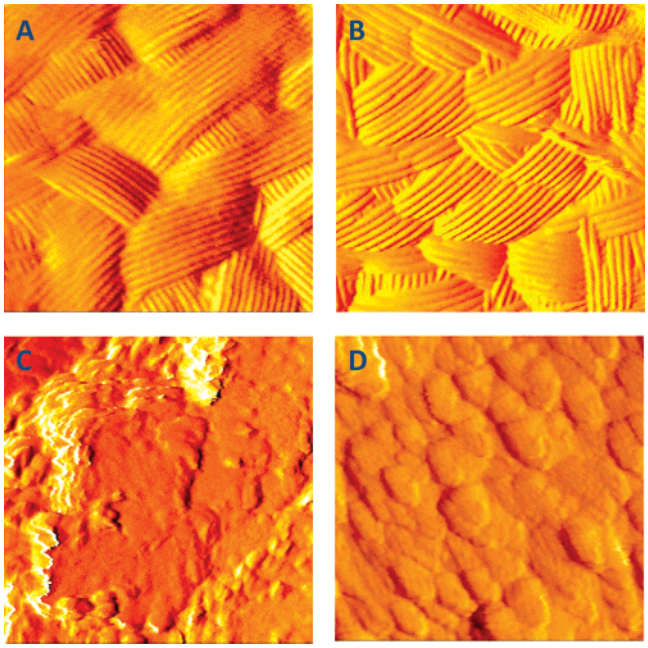

Figure 1. Probing cell surface structure using *in situ* AFM imaging. High-resolution deflection images (500 nm × 500 nm) recorded in deionized water for the surface of *A. fumigatus* conidia: (A) wild type, (B) ΔrodB mutant, (C) ΔrodA mutant, and (D) ΔrodAΔrodB double mutant.

The total intensity (I_{total}) of a spectrum as used in the results section corresponds to the total secondary ion intensity from which the hydrogen peak intensity was subtracted (mass range: $2 \leq m/z < 2000$).

Results and Discussion

Knowledge of the surface properties of *A. fumigatus* conidia is a key to understand their functions, particularly their adhesion to host cells during infection. To gain a comprehensive picture of the structural and chemical properties of *A. fumigatus*, wild-type conidia and three mutants (ΔrodA, ΔrodB, and ΔrodAΔrodB) were analyzed using *in situ* AFM topographic imaging, combined with XPS and SIMS chemical analyses. Previous scanning electron microscopy (SEM) studies revealed that the ΔrodB mutant deficient for the RodBp hydrophobin produces rodlets that are morphologically similar to those of the wild-type, while the ΔrodA mutant deficient for RodAp hydrophobins completely lacks any rodlet.[21,22] This suggested that, unlike RodAp, RodBp is not required for rodlet formation.

With this in mind, we first investigated the surface structure of the different conidia using high-resolution AFM imaging. To this end, the cells were immobilized on polymer membranes, a method which allows live cells to be imaged by AFM without using any drying or fixation procedure.[16] As can be seen in Figure 1, high-resolution images revealed the presence of rodlets, several hundreds nanometers in length and 10 ± 1 nm in diameter, on the surface of the wild-type and of the ΔrodB mutant. By contrast, the surfaces of the ΔrodA mutant and the ΔrodAΔrodB double mutant lacked rodlet structures and were rather granular, presumably reflecting the presence of underlying cell wall polysaccharides (such as chitin, glucan, and galactomannan) and melanin. These *in situ* images are fully consistent with earlier SEM images showing that disruption of the RodA gene, but not of the RodB gene, leads to rodletless surfaces, and thus further strengthen the notion that only RodA is required for rodlet formation. Interestingly, the surface morphologies of the ΔrodA and ΔrodAΔrodB mutants were not identical, suggesting that the RodB gene plays a role in controlling the surface architecture of the cell wall.

Table 1. Surface Chemical Composition Measured by XPS and Proportions of Carbon Involved in Proteins, Polysaccharides, and Lipids Deduced from the Data

strain	% C	% O	% N	N/C	O/C	% C_{Pr}	% C_{Ps}	% C_{Lp}
WT	65.9	26.0	7.9	0.12	0.39	29	20	17
ΔrodB	68.9	21.4	9.4	0.14	0.31	35	12	22
ΔrodA	70.6	23.6	5.7	0.08	0.33	21	20	30
ΔrodAΔrodB	67.4	28.2	4.2	0.06	0.42	15	28	24

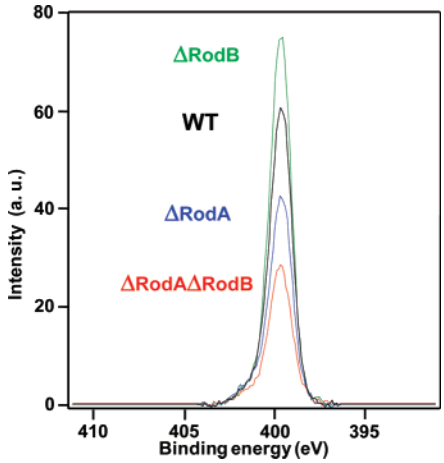

Figure 2. Analysis of the cell surface chemical composition using XPS. Representative N_{1s} spectra obtained for the *A. fumigatus* wild type and ΔrodB, ΔrodA, and ΔrodAΔrodB mutants.

Next, the surface chemical composition of the conidia was determined by XPS. Table 1 presents the surface composition, in terms of mole fraction and atomic concentration ratios with respect to total carbon, determined on the wild-type and on the three mutants. A duplicate set of determinations yielded similar data. Consistent with the general biochemical composition of fungal cell walls, the main elements that were detected were C_{1s}, O_{1s}, and N_{1s}. The carbon peaks (not shown) generally showed three components, attributed to carbon bound only to carbon and hydrogen (binding energy of 284.8 eV), to carbon singly bound to oxygen or nitrogen, including ether, alcohol, amine, and amide (binding energy of 286.3 eV), and to carbon making one double bond or two single bonds with oxygen, including amide, carbonyl, carboxylate, ester, acetal, and hemiacetal (binding energy of 288.0 eV). The broad oxygen peak showed two components, with one attributed to hydroxide, acetal, and hemiacetal (binding energy around 532.7 eV) and the second attributed to oxygen making a double bond with carbon in carboxylic acid, carboxylate, ester, carbonyl, or amide (binding energy around 531.4 eV). Nitrogen appeared at 399.9 eV, which is attributable to unprotonated amine or amide functions (Figure 2). While all conidia showed similar amounts of carbon and oxygen, major differences in the nitrogen content were noted, with the wild-type and ΔrodB mutant being much richer in nitrogen compared to the two other mutants. This difference is also illustrated in Figure 2 by the shapes of the nitrogen (N_{1s}) spectra.

The XPS data were further processed to extract information on the biomolecular composition of the surfaces.[2] The major constituents of the conidial cell walls are polysaccharides (chitin, glucan, and galactomannan) and proteins (hydrophobins), together with some lipidlike compounds. Therefore, the surface composition was modeled in terms of three classes of basic constituents, that is, polysaccharides (Ps), proteins (Pr), and lipids (Lp). Compounds such as lipoproteins were considered as a combination

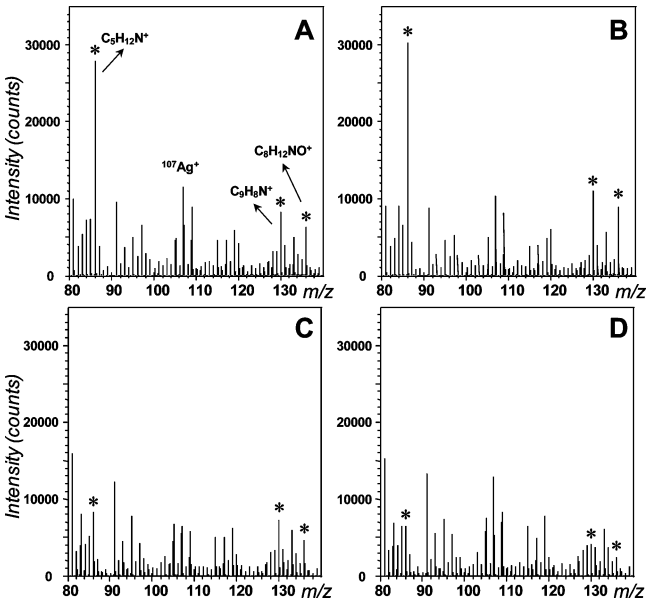

Figure 3. Analysis of the cell surface chemical composition using ToF-SIMS. Positive secondary ion mass spectra obtained for *A. fumigatus* conidia: (A) wild type, (B) ΔrodB mutant, (C) ΔrodA mutant, and (D) ΔrodAΔrodB double mutant. Peaks clearly representative of amino acids are marked by stars.

of basic constituents, namely, lipids plus proteins. The chemical composition of model constituents corresponded to $C_6H_{10}O_5$ for polysaccharides and to CH_2 for lipids, while the amino acid composition considered for proteins was that of a microbial protein.[2]

The molecular composition was computed with the following elemental concentration ratios:

$$[N/C]_{obs} = 0.279(C_{Pr}/C)$$

$$[O/C]_{obs} = 0.325(C_{Pr}/C) + 0.833(C_{Ps}/C)$$

$$[C/C]_{obs} = (C_{Pr}/C) + (C_{Ps}/C) + (C_{Lp}/C) = 1$$

Solving this system of equations provided the proportion of carbon associated with each molecular constituent: (C_{Ps}/C), (C_{Pr}/C), and (C_{Lp}/C). In the light of these proportions, significant differences were observed in the protein and polysaccharide contents when comparing the different strains. First, the wild-type and ΔrodB mutant were substantially richer in proteins than the ΔrodA mutant and the ΔrodAΔrodB double mutant, which is fully consistent with the occurrence of rodlets as observed by AFM. Second, polysaccharides were detected on all strains and thus also on the rodlet-coated wild-type and ΔrodB mutant, which may reflect carbohydrates either buried under the rodlet layer or exposed on its surface.

Last, we probed the surface chemistry of the conidia using ToF-SIMS. Figure 3 shows a portion of the positive secondary ion mass spectra obtained for the wild-type and the three mutants, illustrative of the presence of amino acids on the surfaces. Previously, secondary ion mass spectra peaks that are characteristic of given amino acids were identified.[25,26] The main fragment peaks and their attributions were as follows: $m/z = 30$, CH_4N^+ (glycine and others); $m/z = 44$, $C_2H_6N^+$ (alanine, leucine,

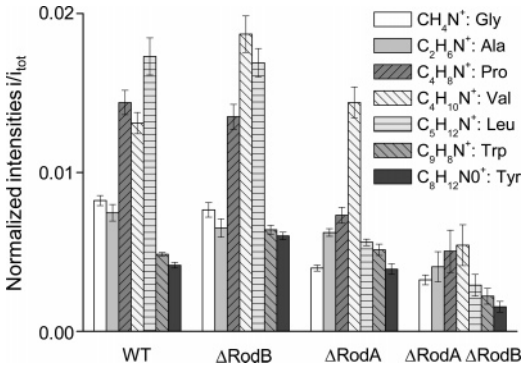

Figure 4. Detection of specific amino acids using ToF-SIMS. Normalized intensities of the characteristic peaks of amino acids detected in the positive mass spectra of the four *A. fumigatus* conidia.

and arginine); $m/z = 70$, $C_4H_8N^+$ (proline); $m/z = 72$, $C_4H_{10}N^+$ (valine); $m/z = 86$, $C_5H_{12}N^+$ (leucine); $m/z = 130$, $C_9H_8N^+$ (tryptophan); $m/z = 136$, $C_8H_{12}NO^+$ (tyrosine).

Figure 4 compares the normalized intensities (see Materials and Methods section) of the amino acid peaks obtained for the four different conidia. Major differences were observed and found to qualitatively correlate with the XPS and AFM data. First, compared to the wild-type, the ΔrodB mutant was richer in three amino acids, essentially valine but also tryptophan and tyrosine, while the other four amino acids were present in similar amounts. Second, the ΔrodA mutant showed smaller amounts of glycine, alanine, proline, and leucine than the wild type, in agreement with XPS (less proteins) and AFM (rodletless surface) data. This finding suggests that rodlets are rich in these four amino acids, which is consistent with the biochemical composition of hydrophobins. Indeed, according to Thau et al.,[21] the RodAp hydrophobin contains 12% glycine, 11% alanine, 10% leucine, and 4% proline, meaning these four amino acids represent almost 40% of the whole protein. Interestingly, we note that the fact that these amino acids are hydrophobic is consistent with a recent chemical force microscopy study revealing the strong hydrophobic character of *A. fumigatus* rodlets.[27] Third, in line with the XPS and AFM data, the ΔrodAΔrodB double mutant showed a dramatic decrease in the concentrations of the seven amino acids.

The above trends were further supported by considering the relationships between the SIMS negative ion intensities and the proportions of carbon associated with proteins and polysaccharides obtained by XPS (Figure 5). Figure 5a shows an excellent correlation between the intensity of the CN^- ion, a generic fragment found in all amino acid spectra, and the amount of carbon involved in proteins (% C_{Pr}) derived from XPS. Even though the information depth of XPS is several times greater than that of SIMS for the considered signals and experimental conditions, the measured correlation is close to linearity. Such a linear relationship is consistent with a distribution of protein "patches" rather than a uniform ultrathin layer which should lead to a power function in Figure 5a.[28] Clearly, SIMS and XPS were consistent in showing more proteins on the ΔrodB mutant and less proteins on the ΔrodA and ΔrodAΔrodB mutants. Because of their high oxygen content, polysaccharides also exhibit characteristic peaks in the negative SIMS spectra, for example, $m/z = 45$ (CHO_2^-) and $m/z = 59$ ($C_2H_3O_2^-$). The evolution of the normalized intensity of the $C_2H_3O_2^-$ peak, reported in Figure 5b, as a function of the amount of carbon involved in

(25) Bartiaux, S. Undergraduate Thesis, Unité de Chimie des Interfaces UCL, Louvain-la-Neuve, 1995.
(26) Lhoest, J. B.; Detrait, E.; van den Bosch de Aguilar, P.; Bertrand, P. *J. Biomed. Mater. Res.* **1998**, *41*, 95.
(27) Dague, E.; Alsteens, D.; Latge, J. P.; Verbelen, C.; Raze, D.; Baulard, A. R.; Dufrêne, Y. F. *Nano Lett.* **2007**, *7*, 3026.
(28) Delcorte, A.; Bertrand, P.; Arys, X.; Jonas, A. *Surf. Sci.* **1996**, *366*, 149.

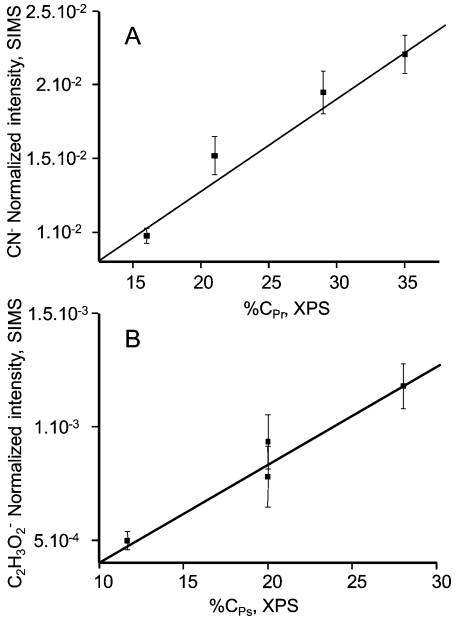

Figure 5. Correlations between XPS and SIMS data. (A) Protein content: correlation between the intensity of the CN^- SIMS peak and the amount of carbon associated with proteins deduced from the XPS data. (B) Polysaccharide content: correlation between the intensity of the $C_2H_3O_2^-$ SIMS peak and the amount of carbon associated with polysaccharides deduced from the XPS data.

polysaccharides (%C_{Ps}) calculated from XPS clearly supports the conclusion that polysaccharides dominate in the ΔrodAΔrodB double mutant while they are depleted in the ΔrodB mutant. The two correlations in Figure 5 also indicate that matrix effects, for example, molecular ion suppression or enhancement due to the molecular environment,[29] do not dominate the SIMS results. Taken together, our data indicate that both the RodA and RodB genes clearly play distinct roles in modulating the nature and the amount of proteins at the conidial surface.

(29) Jones, E. A.; Lockyer, N. P.; Vickerman, J. C. *Appl. Surf. Sci.* **2006**, *252*, 6727.

In conclusion, we have shown the great potential of combining three advanced surface analysis techniques, AFM, XPS, and SIMS, for probing microbial cells. A good agreement between the three methods is demonstrated, even though they have very different operating conditions, probing depth, and lateral resolution. AFM provides topographic images of the outermost surface of hydrated live cells with nanoscale lateral resolution, while XPS and SIMS provide chemical information on dried cells with poor lateral resolution. XPS probes elemental and functional groups over a depth of ∼5 nm and can even provide information on biomolecular constituents. Owing to its much higher surface sensitivity, SIMS provides a semiquantitative chemical analysis of the outermost molecular layers. XPS and SIMS spectra demonstrate that the surfaces of wild-type *A. fumigatus* conidia are fairly rich in proteins, reflecting essentially the rodlet structures seen in the AFM images. In addition, the SIMS data confirm that rodlets are rich in four hydrophobic amino acids, that is, glycine, alanine, proline, and leucine, in agreement with the known amino acid composition of RodAp hydrophobins. The ΔrodB mutant is richer in proteins, particularly in valine, tryptophan, and tyrosine, and also shows rodlets, confirming that the RodB gene is not associated with rodlet production but plays a role in controlling the cell surface composition. By contrast, both XPS and SIMS show that the rodletless ΔrodA and ΔrodAΔrodB mutants are substantially poorer in proteins and richer in polysaccharides, reflecting the occurrence of cell wall carbohydrates.

Acknowledgment. P. Bertrand is gratefully acknowledged for providing access to the ToF-SIMS instrument. The authors also wish to thank M. Henry for helpful comments and discussions. This work was supported by the National Foundation for Scientific Research (FNRS), the Université Catholique de Louvain (Fonds Spéciaux de Recherche), the Federal Office for Scientific, Technical and Cultural Affairs (Interuniversity Poles of Attraction Programme), the Région wallonne (NANOTIC program), the Research Department of the Communauté française de Belgique (Concerted Research Action), and the European STREP LSHB-CT-2004-511952. Y.F.D. and A.D. are Research Associates of the FNRS.

LA703741Y